# Modelling and operation of sub-miniature constant temperature hot-wire anemometry



2016 Meas. Sci. Technol. 27 125301

(http://iopscience.iop.org/0957-0233/27/12/125301)

IOP Publishing Measurement Science and Technology
Meas. Sci. Technol. **27** (2016) 125301 (14pp) doi:10.1088/0957-0233/27/12/125301

# Modelling and operation of sub-miniature constant temperature hot-wire anemometry

**M Samie[1], J H Watmuff[2], T Van Buren[3], N Hutchins[1], I Marusic[1], M Hultmark[3] and A J Smits[3]**

[1] Department of Mechanical Engineering, University of Melbourne, Victoria 3010, Australia
[2] School of Engineering, RMIT University, Melbourne, VIC 3000, Australia
[3] Department of Mechanical and Aerospace Engineering, Princeton University, Princeton, NJ 08544, USA

E-mail: m.samie@student.unimelb.edu.au

Received 4 August 2016, revised 14 September 2016
Accepted for publication 27 September 2016
Published 21 October 2016


**Abstract**

High-Reynolds number flows are very common in technological applications and in nature, and hot-wire anemometry is the preferred method for measuring the time-series of fluctuating velocity in such flows. However, measurement of very high-Reynolds number flows requires hot-wires with higher temporal and spatial resolution than is available with conventional probes. Much effort has therefore been devoted to decreasing the size of the hot-wire probes and this has led to associated challenges with operation. It is this latter operation problem which is the focus of this paper. To this end, an existing theoretical model of constant-temperature hot-wire anemometers (Perry 1982 *Hot-Wire Anemometry* (New York: Oxford University Press), Watmuff 1995 *Exp. Therm. Fluid Sci.* **11** 117–34) is applied, and its accuracy is tested for the first time by comparison to measurements using an in-house constant temperature anemometer (CTA) for both conventional 5 $\mu$m-diameter wires and sub-miniature hot-wires. With the aid of this model, we propose modifications to the CTA design and demonstrate successful operation of the CTA with the Princeton nano-scale thermal anemometry probe (NSTAP) (Bailey *et al* 2010 *J. Fluid Mech.* **663** 160–79). It is also shown that the transfer function obtained from the model can be utilized to estimate the true frequency response and cut-off frequency of a hot-wire-CTA system to the velocity fluctuations, which is essential in accurate measurements of energy spectrum and higher order statistics of turbulent flows.

Keywords: sub-miniature wire, hot-wire anemometry, high-Reynolds number flows

(Some figures may appear in colour only in the online journal)

## 1. Introduction

Studying high-Reynolds number boundary layer flows has improved extensively over the past few decades thanks largely to the construction and development of high Reynolds number experimental facilities [4–9]. In conjunction with this, advances in sub-miniature hot-wire ($l < 100$ $\mu$m) anemometry have also been required in order to capture the smallest scales of motions in these flows. For wall-bounded turbulent flows, the Reynolds number based on friction velocity, $\mathrm{Re}_\tau = \frac{u_\tau \delta}{\nu}$, represents the ratio of the largest scale size, which is proportional to the boundary layer thickness in turbulent boundary layer flows and pipe radius in pipe flows ($\sim\delta$), to the smallest scale, which is given by viscous length scale ($\sim\frac{\nu}{u_\tau}$). $\mathrm{Re}_\tau$ can exceed $10^5$ in high-Reynolds-number flows which means that in a laboratory facility with fixed dimensions, the small-scale eddy size can be of order of micrometers. Using sensors with sizes greater than the smallest scales of motion results in spatial filtering [10]; this filtering issue has been thoroughly investigated for instance by Johansson and Alfredson [11], Willmarth and Sharma [12], Ligrani and Bradshaw [13], Hites [14], and Hutchins *et al* [15]. Conventional hot-wires with a sensing length of 500–1000 $\mu$m are not usually suitable for high-Reynolds number flow studies in existing facilities due to spatial resolution issues.

Temporal resolution is another limit in using hot-wires for measuring velocity fluctuation of high-Reynolds number flows. Hutchins *et al* [15] showed that the maximum frequency

 

content of a wall-bounded turbulent flow spectrum is equal to or greater than $\frac{u_\tau^2}{3\nu}$, meaning that if the experimental measuring system cannot resolve time scales down to $t = \frac{3\nu}{u_\tau^2}$, there will be an excessive temporal filtering of the measured energy, in addition to spatial attenuation. Therefore, there is a direct relationship between Reynolds number and highest frequency of a flow. Typically, hot-wire anemometers have been reported to have frequency responses in the range $30 < f < 100\,\text{kHz}$ which might be insufficient to fully resolve high-Reynolds number flows temporally [15].

A number of notable efforts have been made towards realising adequately small hot-wires, (see e.g. [3, 16–18]) one of the most important of them being the development of the nano-scale thermal anemometry probe, NSTAP [3], which uses MEMS-based technology for the probe construction and results in sensor lengths of order 30–60 $\mu$m. However operating NSTAP and other sub-miniature probes is not straightforward. Currently NSTAP can be operated with the Dantec Streamline anemometer but only using external resistors [19]. That is, this anemometer is not designed for sensors with the high resistance as found with NSTAPs. Attempts to operate NSTAP with other anemometers result in frequent sensor breakages. Moreover, the best possible square-wave test response of NSTAP with the Dantec Streamline anemometer does not resemble a typical optimal square-wave test response of conventional wires as introduced by Freymuth [20] (see [19] for NSTAP square-wave responses). We address the issue of appropriate operation of sub-miniature hot-wires by employing theoretical modelling to optimise an in-house CTA: the Melbourne University constant temperature anemometer (MUCTA) for this purpose.

There are numerous analytical studies in the literature devoted to hot-wire anemometry, e.g. [1, 2, 20–29]. Freymuth [20, 21] derived CTA governing equations in the time domain for a CTA with a single stage amplifier in the feedback circuit. After linearisation Freymuth showed that a well tuned CTA is governed by a third order ODE assuming that the time constant of the hot-wire is much larger than that of the amplifiers and also depicted the square-wave response for a well tuned CTA system. Perry [1] and Perry and Morrison [22] studied the CTA system theoretically and derived the governing equations in the frequency domain proposing a third order transfer function for the linearised case assuming again an idealised single-stage amplifier in the feedback circuit with infinitely flat broadband response. Wood [23] followed Perry and Morrison's [22] approach but used a single stage amplifier with a frequency dependent transfer function and a lumped inductance in the Wheatstone bridge. This system was controlled by changing the amplifier gain and bridge compensation inductance rather than the amplifier offset voltage used by Perry and Morrison [22]. Wood [23] compared this theoretical model with a DISA 55D01 square-wave response and observed that the model could not accurately predict the anemometer's square-wave response. Watmuff [2] expanded Perry's model and analysed a general CTA in the frequency domain with multiple amplifier stages with frequency dependent transfer functions and also considered the general impedance for bridge components. The analysis of Watmuff shows that a minimum of two equivalent amplifier stages are required to properly account for the introduction of offset voltage perturbations. This is a key point, because the poles of the amplifier which precede the offset voltage injection stage appear as zeros in the overall system transfer function for offset voltage fluctuations. Watmuff's study was limited to analysis, and did not involve validation against real CTAs.

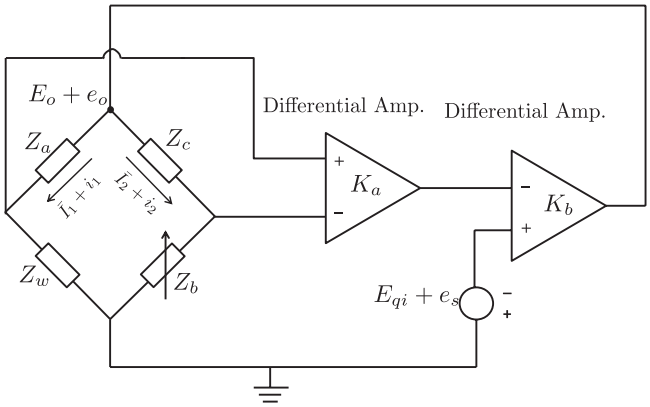


**Figure 1.** Model of CTA circuit.

Despite all the above-mentioned studies and the noted difficulties associated with operation of sub-miniature wires, interaction of these wires with the CTA has not been studied sufficiently to the best of the authors' knowledge, which is vital today due to the increasing need for employing smaller and smaller wires for studying high-Reynolds number flows. An exception is the study by Watmuff [2] in which he briefly discussed stability conditions of sub-miniature wires, showing that a higher cut-off frequency and gain of amplifiers is required for stable operation of sub-miniature wires than for larger wires. In the present study we first evaluate Watmuff's model by comparing its results against experiment, then employ it to investigate the operation of sub-miniature wires with CTAs more comprehensively.

## 2. Theory

In this section the theoretical model developed by Watmuff [2] is presented briefly.

### 2.1. Static analysis

Figure 1 shows a typical CTA circuit. It consists of a Wheatstone bridge in which the hot-wire ($Z_w$) is one of the arms of the bridge, and impedances $Z_a$, $Z_b$, and $Z_c$ form the other arms. Feedback includes two amplifiers with DC gains of $K_a$ and $K_b$ and an offset voltage $E_{qi}$ applied to the second amplifier. The static electric current passing through the wire $\bar{I}_1$ needs to be determined first since it is required in dynamic analysis. Only resistive component of the impedances need to be considered in the static analysis, i.e. $Z_w = \overline{R_w}$, $Z_a = R_a$, $Z_b = R_b$, and $Z_c = R_c$. A static circuit analysis determines $\bar{I}_1$ as follows.

$$\bar{I}_1 = \frac{K_b E_{qi}(R_b + R_c)}{(R_b + R_c)[R_a + (\overline{R_w} + R_l)] + K_a K_b \dot{R}} \qquad (1)$$

where $\dot{R} = [(\overline{R_w} + R_l)R_c - R_aR_b]$, $\overline{R_w}$ (still unknown) is the hot-wire's static operating resistance, and $R_l$ is the sum of resistances of the stubs (un-etched part of the wire) and wire connectors to the circuit.

The mean temperature of the wire (which is constant throughout the operation) is the result of balancing the Joule heating and heat convected by the flow over the wire (axial heat conduction is neglected here for simplicity). If the equation recommended by Kramers [30] is used for Nusselt number (assuming $Pr = 0.7$ for air) another equation relating hot-wire current and resistance will be given as

$$\bar{I}_1^2 = (1 - \frac{R_g}{\overline{R_w}})(\frac{\pi k_g l}{CR_0})(0.39 + 0.51\sqrt{\frac{\mathrm{d}U}{\nu_g}}) \tag{2}$$

In equation (2), $R_g$ is the wire resistance at the gas temperature, $k_g$ is the gas conductivity, $l$ is the wire length, $d$ is the wire diameter, $C$ is the resistance temperature coefficient of the wire, $\nu_g$ is the gas viscosity, $R_0$ is the wire resistance at the reference temperature, and $U$ is the mean gas velocity past the wire. By solving equations (1) and (2), $\bar{I}_1$ and $\overline{R_w}$ are obtained and the static operating point is determined. It is noteworthy that $\overline{R_w}$ is not determined only by bridge resistors since the bridge is not usually in perfect balance, i.e. $(\overline{R_w} + R_l)R_c - R_aR_b \neq 0$. It is clear from equations (1) and (2) that $K_b$, $K_a$, and $E_{qi}$ contribute to the operating point as well as $R_a$, $R_b$, and $R_c$. Hence by changing offset voltage $E_{qi}$, hot-wire resistance $\overline{R_w}$ and overheat ratio $R = \frac{\overline{R_w}}{R_g}$ vary. The overheat ratio dictates the static operating temperature of the wire.

### 2.2. Dynamic analysis[3]

In order to analyse the dynamic behaviour of a CTA, a square-wave test is used to optimise its frequency response. A square-wave signal is applied to a specific point of the feedback circuit (second stage differential amplifier here) and by tuning the circuit, the best frequency response is obtained. It has been shown that a square-wave test, if appropriately interpreted, can be representative of the CTA response to the velocity fluctuations [1, 2, 20, 29]. Hence, a voltage perturbation analysis is essential in order to gain a comprehensive understanding of the dynamic behaviour of CTA.

The dynamic circuit equations of the circuit shown in figure 1 can be written as follows:

$$e_o = Z_a i_1 + e_w \tag{3}$$

$$e_o = (Z_c + Z_b)i_2 \tag{4}$$

$$e_o = [(Z_b i_2 - e_w)K_a\frac{A_a(s)}{B_a(s)} - e_s]K_b\frac{A_b(s)}{B_b(s)} \tag{5}$$

where $Z_a$, $Z_b$, and $Z_c$ are the Wheatstone bridge arm impedances, $e_w$ is the wire's voltage fluctuation, $e_o$ is the output voltage fluctuation, $i_1$ and $i_2$ are fluctuations of the electric currents of Wheatstone bridge arms shown in figure 1, and $e_s$ is voltage fluctuation injected to the offset voltage node, i.e. square-wave applied to the second amplifier. In our circuit analysis differential amplifiers are treated with the governing equation $e_{o_i} = K_i\frac{A_i(s)}{B_i(s)}\Delta e_i, (i = a, b)$ where $K_i$ is amplifier's DC gain, $A_i(s)$ and $B_i(s)$ are polynomials for the zeros and the poles in the transfer function of the amplifiers respectively, $\Delta e_i$ is amplifier's input voltage difference, and $e_{o_i}$ is its output voltage. When a square-wave test is conducted, velocity fluctuations are absent and the wire voltage fluctuation is

$$e_w = i_1\overline{R_w} + \bar{I}_1 r_w = i_1 Z_w \tag{6}$$

where $Z_w$ is wire impedance and a lumped model is used, following Perry [1]. By combining equations (3)–(6) and after some manipulation, the voltage fluctuation transfer function of the CTA is obtained as

$$\frac{e_o}{e_s} = \frac{B_a(s)}{K_a A_a(s)P(s)} \tag{7}$$

where

$$P(s) = \frac{Z_b}{Z_b + Z_c} - \frac{Z_w}{Z_w + Z_a} - \frac{B_a(s)B_b(s)}{K_a K_b A_a(s)A_b(s)} \tag{8}$$

When velocity fluctuations are measured by the hot-wire, offset voltage fluctuations are absent, i.e. $e_s = 0$. Perry [1] showed that voltage fluctuations of a constant temperature wire exposed to velocity fluctuations to the linearised approximation is

$$e_w = \frac{\partial E_w}{\partial U}u + \frac{\partial E_w}{\partial I}i \tag{9}$$

where $u$ and $i$ are velocity and electric current fluctuations respectively, $\frac{\partial E_w}{\partial I} = Z_w$, and $\frac{\partial E_w}{\partial U}$ depends on the adopted wire heat transfer relation. In this study we use equation recommended by Kramers [30] for the wire heat transfer.

By combining equations (3)–(5) and (9), and remembering that $e_s = 0$, the velocity fluctuations transfer function is determined as

$$\frac{e_o}{u} = \frac{\frac{Z_a}{Z_w + Z_a}\frac{\partial E_w}{\partial U}}{P(s)} \tag{10}$$

where $P(s)$ is introduced in equation (8).

**Table 1.** Dimensions of the probes used in this study. $l_w$ is the sensing element length, $d_w$ is the hot-wire sensing element diameter, $l_s$ and $d_s$ are the hot-wire stub length and diameter respectively, and $w_w$ and $t_w$ are the NSTAP probe sensing element width and thickness respectively.

| | $l_w$ ($\mu$m) | $d_w$ ($\mu$m) | $l_s$ ($\mu$m) | $d_s$ ($\mu$m) | $w_w$ ($\mu$m) | $t_w$ ($\mu$m) |
|---|---|---|---|---|---|---|
| HW1 | 1000 | 5 | 1000 | 40 | — | — |
| HW2 | 500 | 2.5 | 500 | 50 | — | — |
| HW3 | 250 | 1 | 625 | 30 | — | — |
| NSTAP | 60 | — | — | — | 2 | 0.1 |

[3] In this paper the governing differential equations are written using Laplace transforms. To have the equations in terms of frequency, the Laplace variable $s$ is simply replaced by $j\omega$ where $j = \sqrt{-1}$ and $\omega$ is angular frequency.

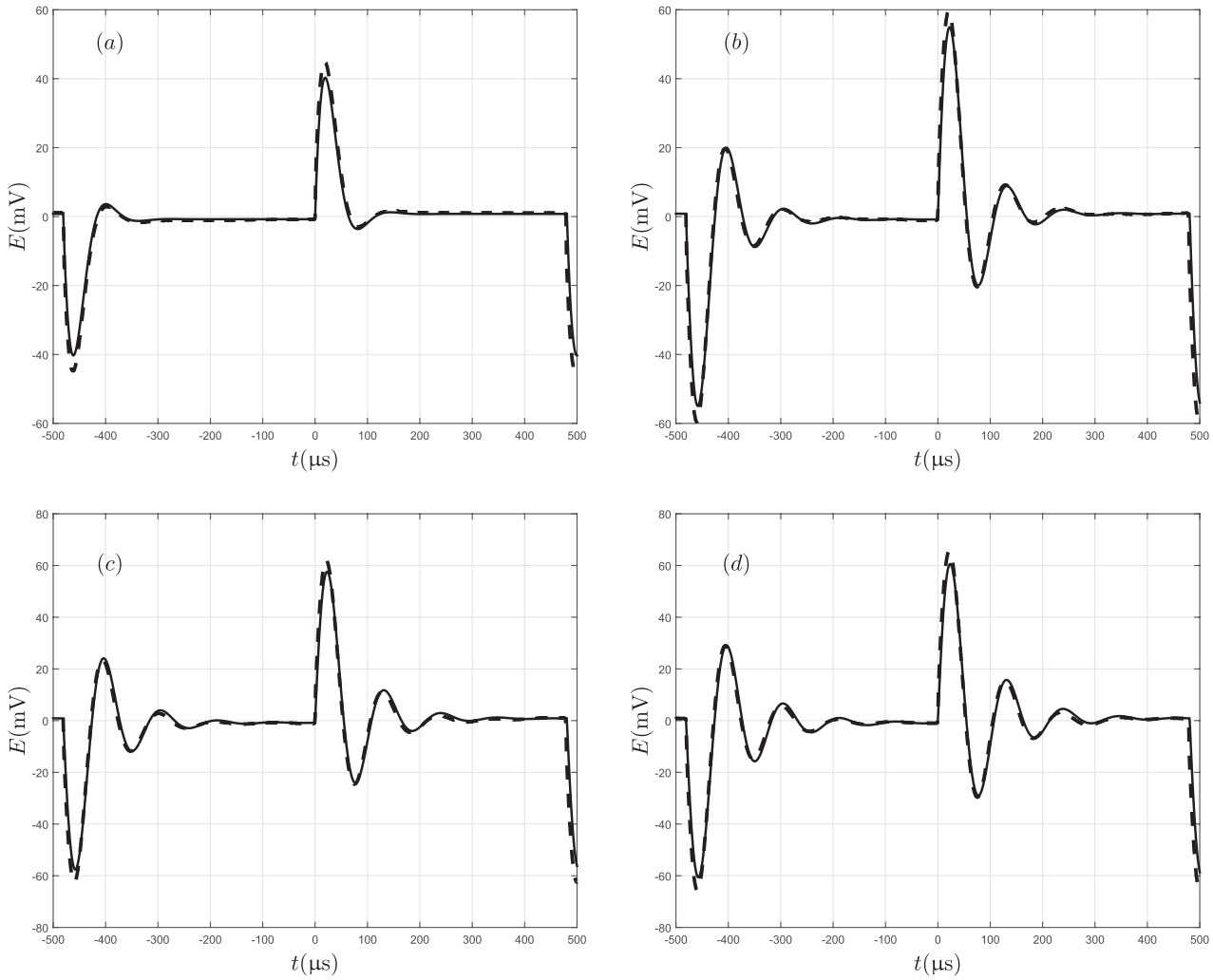


**Figure 2.** Comparison between theory and experiment for the square-wave response of a 5 $\mu$m-diameter wire. A MUCTA is used with $R_a = 100\ \Omega$, $R_b = 120\ \Omega$, $R_c = 1000\ \Omega$, and different offset voltages of (a):1.43 V, (b):0.74 V, (c):0.64 V, (d):0.54 V. The mean flow velocity over the hot-wire is $\bar{U} = 10.5\ \mathrm{ms}^{-1}$. ----: experiment, ——: theoretical model.

If all the parameters are introduced in the polynomial form in equations (7), (8) and (10), after trivial algebra, transfer functions are obtained in rational form. (see [2].)

## 3. Experiments

A set of experiments was conducted to examine the level of accuracy of the analytical model and also to test the possibility of using sub-miniature wires, which has been troublesome due to breakage and also inefficient tuning issues.

Three standard hot-wire probe types along with the sub-miniature NSTAP probes were used throughout the experiments. In the majority of measurements, a Dantec 55P05 boundary layer type probe was used, with prong spacing 3 mm. Wollaston wires were soldered to the prong tips and etched to reveal a 5 $\mu$m-diameter platinum-sensing element of length 1 mm in the middle. The un-etched portions (stubs) are 1 mm in length and have an estimated diameter of 40 $\mu$m. Other hot-wire probe types were Dantec 55P15 boundary layer type with prong spacing 1.5 mm. Wollastan wires with platinum cores of 2.5 and 1 $\mu$m-diameter are used to produce them. The production process is identical to that of the 5 $\mu$m-diameter wires; the etched sensing length is 0.5 mm for 2.5 $\mu$m-diameter and 0.25 mm for 1 $\mu$m-diameter wire. The NSTAP probe had a sensing element consisting of a platinum (Pt) filament measuring 60 $\mu$m $\times$2 $\mu$m $\times$ 100 nm. The dimensions of all the probes used for the experiments are summarised in table 1.

An in-house Melbourne University constant temperature anemometer (MUCTA) designed based on references [1] and [22] was used in the experiments. In the MUCTA a 10:1 ratio Wheatstone bridge is used with $R_a = 100\ \Omega$, $R_c = 1000\ \Omega$, and variable $R_b$ to set the desired overheat ratio. A high performance instrumentation amplifier (simple pole) with DC gain $K_a = 100$ and corner frequency $f \approx 750$ kHz is used as the first stage amplifier and a differential amplifier configuration as the second stage amplifier. By selecting appropriate resistors and capacitors, the desired corner frequency and DC gain of the second stage amplifier can be set.

Validation of the analytical model is presented in the following two sections: 3.1 square-wave test, 3.2 velocity fluctuations.

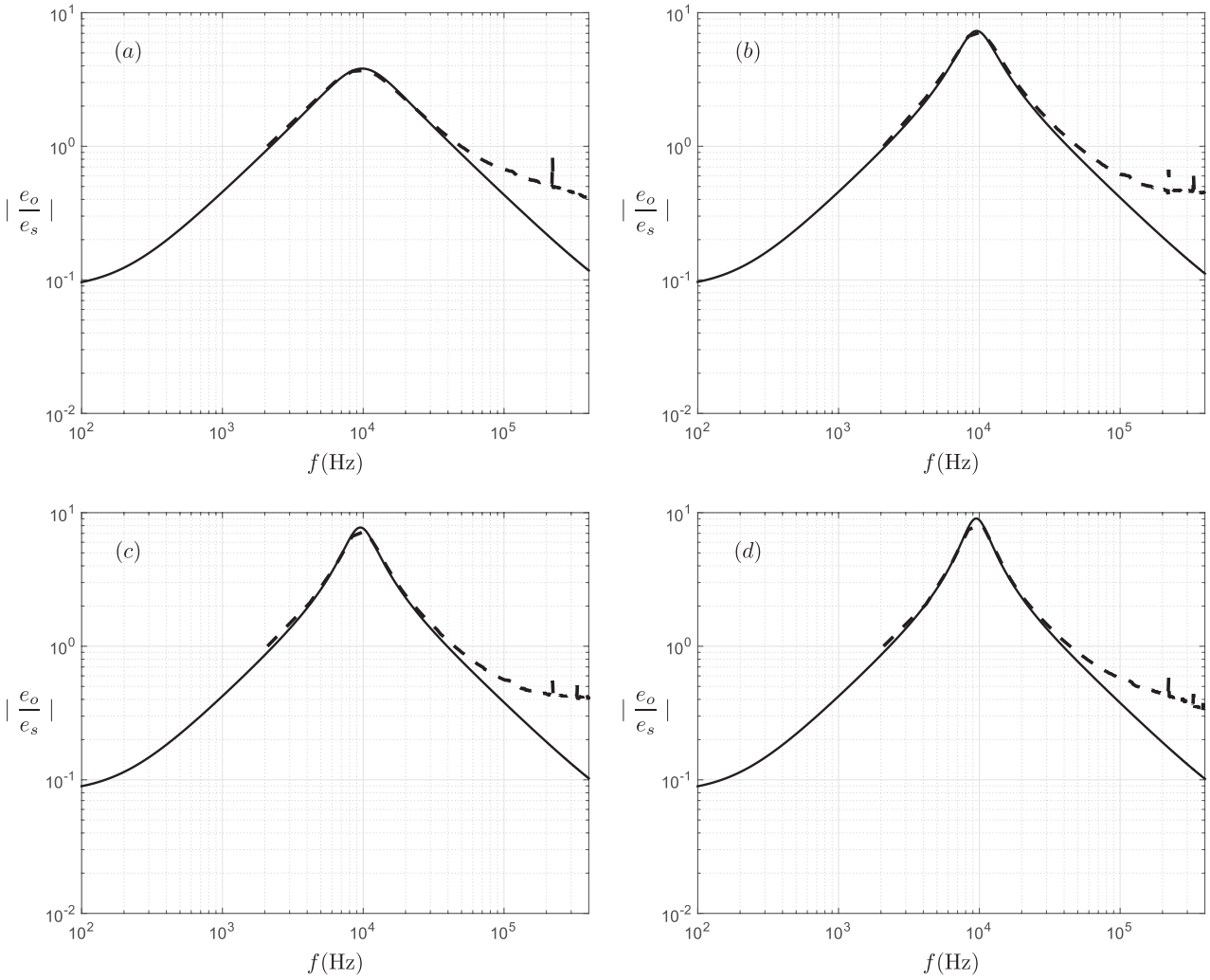


**Figure 3.** Comparison between theoretical and experimental transfer functions for the square-wave responses shown in figure 2. - - - -: experiment, ——: theoretical model.

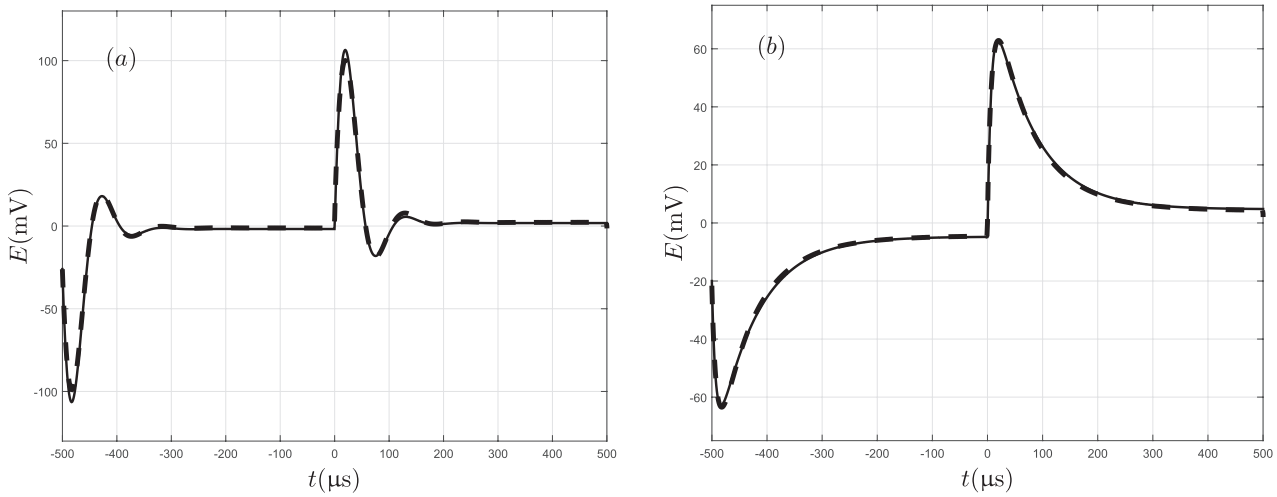


**Figure 4.** Square-wave test response of two tuning conditions used for validating analytical transfer function of velocity fluctuations: (a) slightly under-damped, (b) over-damped. - - - -: experiment, ——: theoretical model.

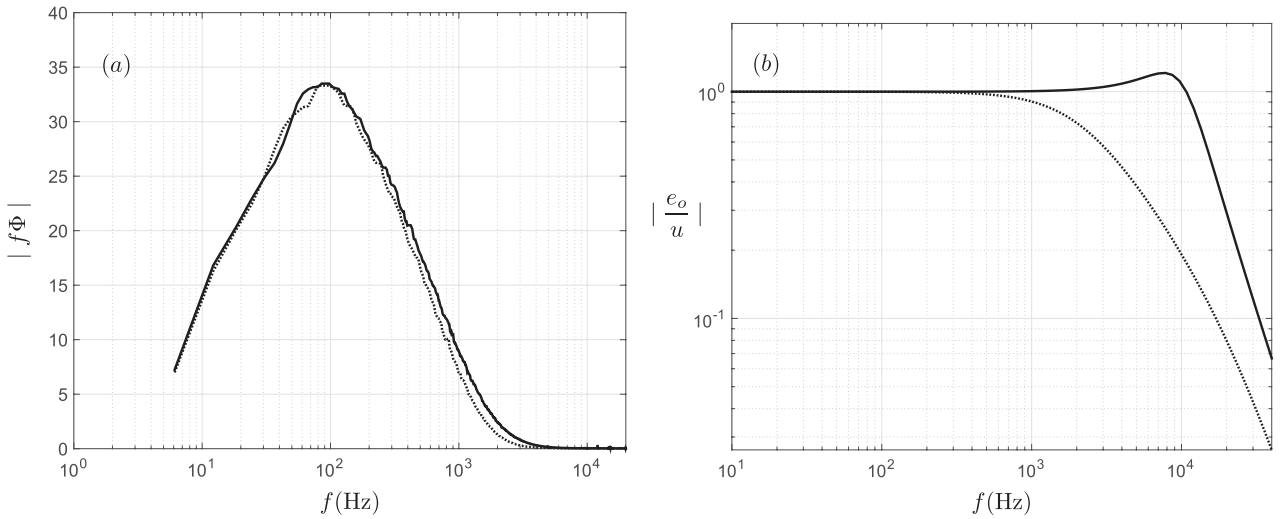


**Figure 5.** (a) Pre-multiplied energy spectra of uncalibrated voltage fluctuations measured by slightly under-damped and over-damped hot-wire-CTA systems at the center of channel. (b)Velocity fluctuation transfer function magnitude as predicted by the theoretical model for two mentioned tunings of the MUCTA used in experiments with pre-multiplied energy spectra shown in a. ——: slightly under-damped condition, ····: over-damped condition.

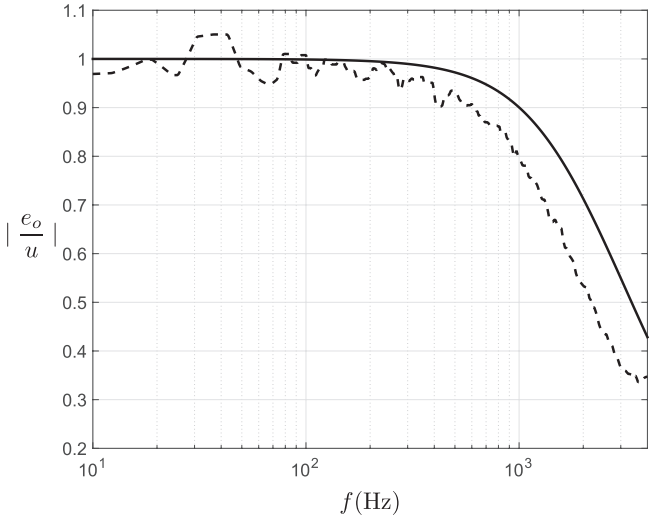


**Figure 6.** Comparison between relative theoretical and experimental velocity transfer functions. - - - -: experiment, ——: theoretical model.

### *3.1. Square-wave test validation*

A 5 $\mu$m-diameter wire was utilized for this test and was located at the centre of a fully turbulent channel flow. A $\sim$1 kHz square-wave with an amplitude of 50 mV was used. Since the core flow of the channel is fully turbulent, the velocity fluctuations, though small, were superimposed on the applied square-wave response. To isolate the square-wave response from the velocity fluctuations, the square wave response was sampled using an A/D board at 1 MHz for 60 s and several thousand response signatures were ensemble averaged. To extract the square-wave response signature, the injected square-wave signal was sampled simultaneously and the risings of the sampled square-wave signal was used to phase average the CTA signal, and produce a conditionally averaged square-wave response.

Several flow velocities and anemometer adjustments were tested in different runs; four of them are presented here in figure 2. The experimentally measured square-wave responses are shown by the dashed lines, while the solid lines show the model prediction. It can be seen that except for a slight difference in the first peak, which is at $t \approx 2 \times 10^{-5}$ s (corresponding to a sinusoid function with frequency of $f \approx 12.5$ kHz), theory and experiment are in excellent agreement. To further investigate these differences one can explore the transfer functions corresponding to the transient responses shown in figure 2. The transfer function of a control system can be obtained experimentally, by taking the Fourier transform of the impulse response of it (which can be obtained by taking derivative of square-wave response of that system). By doing so, the transfer functions of the CTA corresponding to the tests shown in figure 2 are determined and depicted in figure 3. Theoretical and experimental transfer functions are normalized by their magnitude at $f \approx 2.2$ kHz to make comparison between theory and experiment feasible. It can be seen in figure 3 that the experimental transfer functions start to peel off from the theoretical ones at $f \approx 15$ kHz; but agree reasonably well up to $f \approx 40$ kHz, which is the upper bound of the frequency range in which the signal contains most of its energy. The reasons for the discrepancy between the theoretical and experimental square-wave test transfer function observed here will be discussed in section 5.

### *3.2. Validation of transfer function related to velocity fluctuations*

Measuring the direct frequency response of a hot-wire-CTA system to velocity fluctuations is not as easy as the electronic square-wave test, especially up to very high frequencies.

Perry and Morrison [31] exposed a hot-wire to the periodic Karman Vortex streets behind a cylinder. Using this technique they were able to measure their system frequency response up

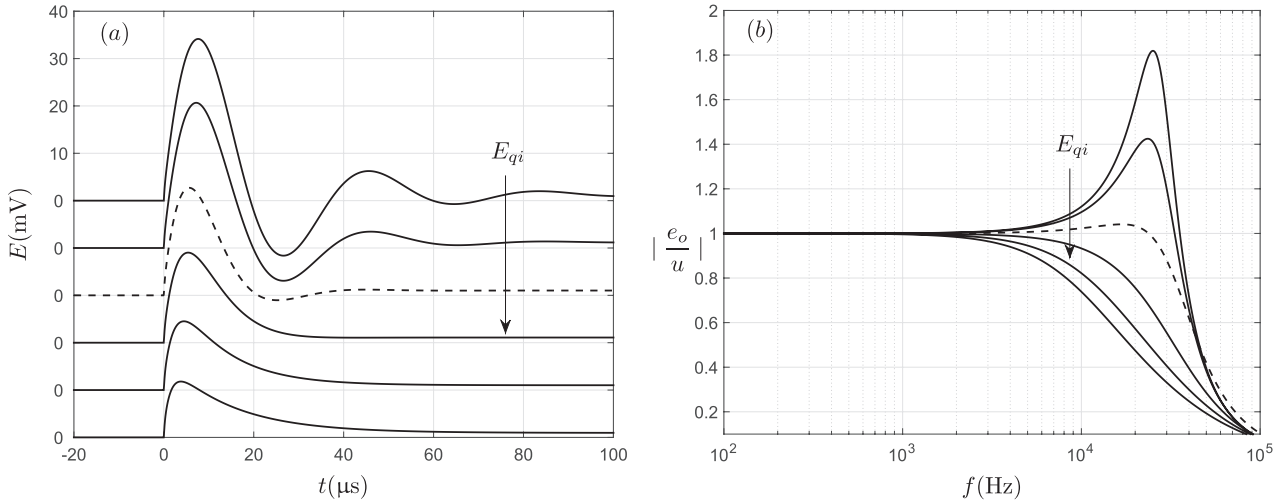


**Figure 7.** Variation of the frequency response of a modelled CTA system with offset voltage $E_{qi}$, operating a conventional 2.5 $\mu$m-diameter (500 $\mu$m-length) wire. Numerical values of the offset voltages are 0.6, 0.8, 1.4, 2, 3, and 4 V and arrow direction indicates increase in offset voltage. Dashed curves correspond to the optimal response. (a) Square-wave response. (b)Velocity transfer function magnitudes corresponding to the square-wave responses in a. Square-wave response curves have been shifted in the ordinate axis for clarity.

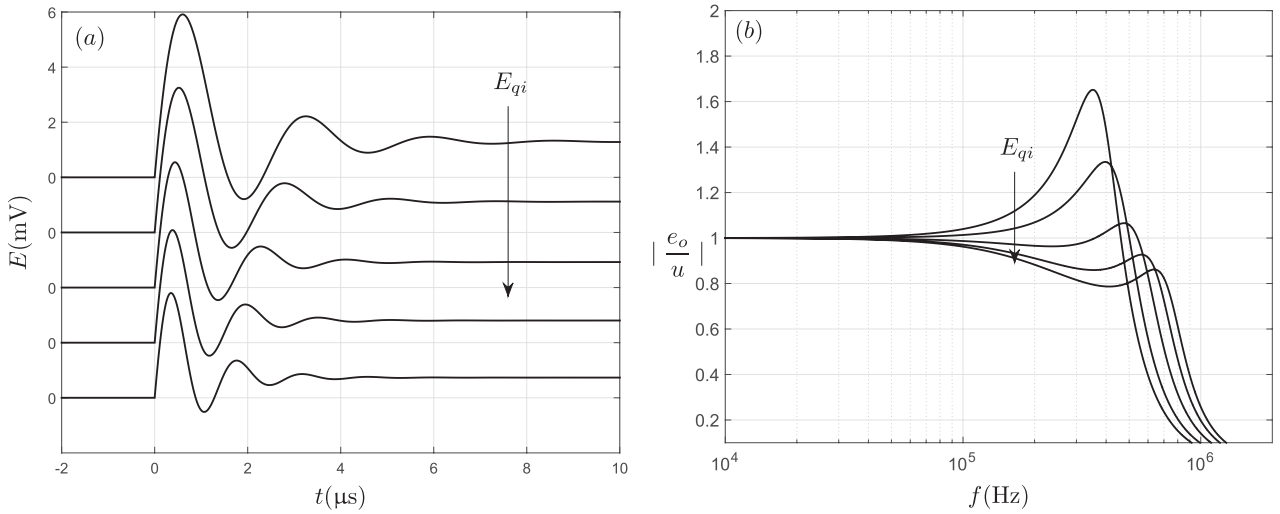


**Figure 8.** Variation of the frequency response of a modelled CTA system with offset voltage $E_{qi}$, operating a 0.2 $\mu$m-diameter (30 $\mu$m-length) wire. Numerical values of offset voltages are 0.8, 1.2, 2, 3, and 4 V and arrow direction indicates its increase. (a) Square-wave response. (b)Velocity transfer function magnitudes corresponding to the square-wave responses in a. Square-wave response curves have been shifted in the ordinate axis for clarity.

to nearly 10 kHz. They observed that their in-house CTA exhibited a flat response to velocity fluctuations up to 10 kHz, while the tested DISA 55A01 anemometer exhibited a 3 dB attenuation at 6 kHz. Khoo *et al* [32] utilized a specially designed apparatus consisting of a top rotating disc with recesses cut on its surface and a bottom stationary disc for providing known velocity fluctuations up to 1600 Hz over the hot-wire. By using this apparatus they observed that a Dantec 56C01 anemometer showed a flat response to velocity fluctuations up to 1600 Hz which is not unexpected at such a relatively low frequency. Hutchins *et al* [33] used a fully developed turbulent pipe flow to create the input velocity fluctuation to the hot-wire. They exploited the unique capabilities of the Princeton Superpipe, in which the kinematic viscosity of the air can be changed via pressurisation, to explore various turbulent pipe flows at matched Reynolds numbers, but with turbulent energy in different frequency ranges. They argued that based on Reynolds similarity, any difference among the normalised energy spectra is due to differences in frequency response of the CTA systems. They used three different anemometers and showed that the frequency response of under- or over-damped CTA systems is approximately flat up to only 5–7 kHz.

Considering the fact that special apparatus is required to carry out direct testing of CTA systems, the proposed velocity transfer function by Watmuff [2] and developed in section 2 proves to be advantageous. However, the accuracy of this model should be assessed first. To this end, a 5 $\mu$m-diameter hot-wire was placed at the center of a turbulent flow channel. The MUCTA was used to operate the wire. Two different tuning conditions (one slightly under-damped and the other over-damped) were examined to measure velocity fluctuations of the flow at the same location. Figure 4 depicts

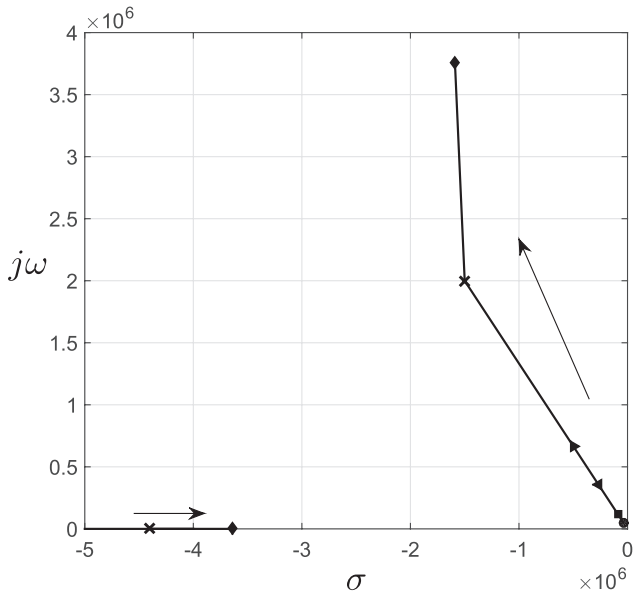


**Figure 9.** Dominant poles of closed-loop transfer function related to the square-wave injection of the modelled CTA combined with 5(●), 2.5(■), 1(◀), 0.6(▶), 0.3(×), and 0.12(◆) $\mu$m-diameter wires. Arrows show decrease in diameter.

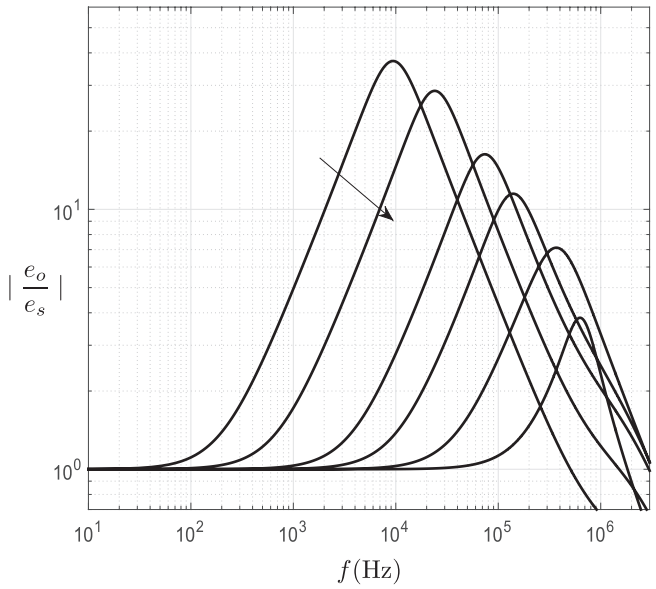


**Figure 10.** Normalized closed-loop transfer function magnitudes related to the square-wave injection of the modelled CTA combined with 5, 2.5, 1, 0.6, 0.3, and 0.12 $\mu$m-diameter hot-wires. Arrow shows decrease in diameter.

square-wave test results for two tunings which are classically considered as slightly under-damped tuning (figure 4(a)) and over-damped (figure 4(b)). Figure 5(a) shows voltage spectra (premultiplied by frequency $f$, so that equal areas equate to equal energy densities on the semilogorithmic plot: $\overline{e_o^2} = \int_0^\infty \Phi \mathrm{d}f = \int_0^\infty f\Phi \mathrm{d}(\log f)$ where $\overline{e_o^2}$ is the variance of the voltage signals and $\Phi$ is energy spectrum of the voltage fluctuations) as measured by the slightly under-damped and over-damped hot-wire systems. The corresponding velocity transfer function magnitudes for two different tunings as calculated by the theoretical model are depicted in figure 5(b). One can see in both plots that the energy spectra and transfer function magnitudes of the two tunings start to diverge at $f \approx 200$ Hz. In order to compare the theoretical transfer function with the real transfer function of two measurement conditions we can use relative transfer functions since real absolute transfer functions cannot be realized without an accurate, known, high frequency velocity fluctuation. The relative experimental transfer function can be obtained by dividing the energy spectrum measured by the over-damped system by the one measured by the under-damped system. Likewise, the relative theoretical transfer function can be obtained by dividing the magnitude of the over-damped transfer function by the magnitude of the under-damped transfer function. Experimental and theoretical relative transfer functions are plotted in figure 6. In general the theoretical relative transfer function captures well the salient characteristics of the experimental system. However, it can be seen that experimental relative transfer function rolls off at a slightly lower frequency than the theoretical one. One reason for this difference might be the simple lumped model for the hot-wire sensor which has been chosen to make the analysis tractable. In the lumped model, conductive heat transfer to the prongs (known as end conduction) and also vibrations of the wire sensor are neglected. Despite the observed discrepancy between theory and experiment for velocity transfer function, the model can be used as a quick reference for estimating the real frequency response of a CTA system in the absence of any other practical methods and also for studying the sensitivities of the velocity transfer function to different tuning settings such as offset voltage, bridge compensation inductance, and amplifier gain and corner frequency.

So far we have shown that the model is able to mimic the operation of conventional hot-wires ($l \approx 500$–$1000$ $\mu$m) with good accuracy. In section 4 we implement the model to demonstrate the behaviour of sub-miniature wires ($l < 100$ $\mu$m) operated with the CTAs designed for conventional wires; and in section 5 we address issues associated with operation of these wires such as frequent hot-wire breakages and stability problems.

## 4. Frequency response of sub-miniature hot-wires

Square-wave tests are used to optimise the frequency response of a CTA system and find its cut-off frequency. The dashed curves in figures 7(a) and (b) show the optimal frequency response of a conventional hot-wire and its corresponding velocity transfer function which are identical to those of an optimally tuned system introduced by Freymuth [20]. A circuit with the following components is modelled in this section: a 10:1 ratio Wheatstone bridge with $R_a = 100\ \Omega$, $R_c = 1000\ \Omega$, and variable $R_b$ (and lumped inductance $L_b$) to adjust overheat ratio (and optimise frequency response) of the sensor. The first stage differential amplifier has a DC gain $K_a = 100$ and a single pole transfer function with cut-off frequency $f_c = 400$ kHz.

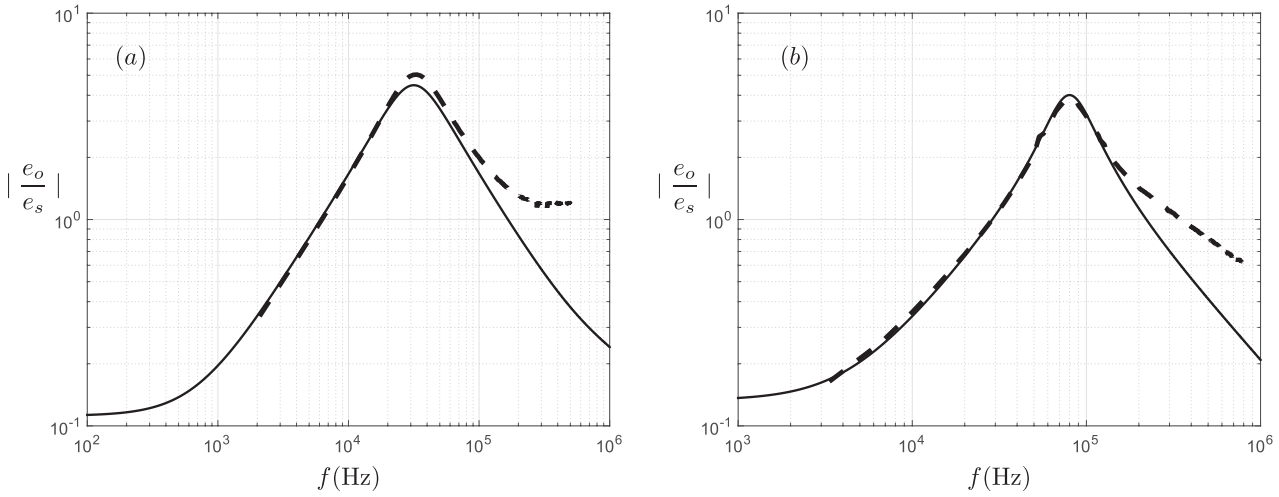


**Figure 11.** Comparison between theoretical and experimental transfer functions for square-wave response of MUCTA before modification (adding the capacitor $C$ to the impedance $Z_4$) with: (a) 2.5 $\mu$m-diameter wire, (b) 1 $\mu$m-diameter wire. ——: theory, - - - -: experiment.

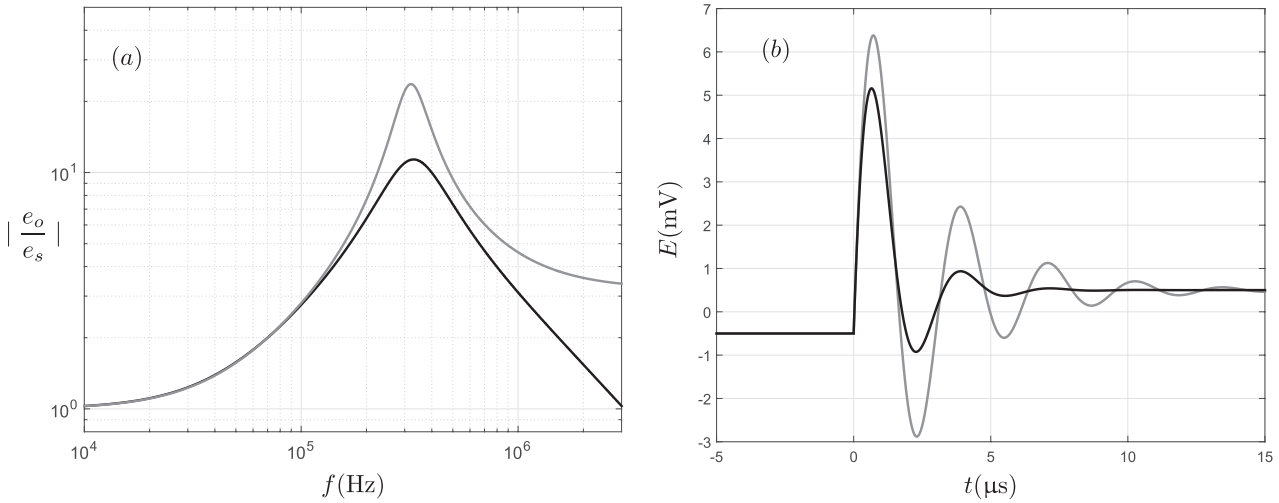


**Figure 12.** (a) Theoretical (——) and synthetic (——) electric test transfer function for the MUCTA operating a 0.3 $\mu$m-diameter hot-wire before modification (adding the capacitor $C$ to the impedance $Z_4$), (b) their corresponding square-wave time response.

The Second stage amplifier is a differential amplifier having DC gain $K_b = 10$ and single pole transfer function with cut-off frequency $f_c = 15$ kHz. The circuit is combined with a 2.5 $\mu$m-diameter (500 $\mu$m-length) wire. Different adjustments by changing the offset voltage $E_{qi}$ are tested and the square-wave responses and the corresponding velocity transfer function magnitudes are shown in figure 7. The response curves are shifted in the ordinate axis for clarity. It can be seen that by increasing the offset voltage, the response of the CTA system becomes increasingly damped. The same circuit is modelled to operate a 0.2 $\mu$m-diameter (30 $\mu$m-length) wire and the results are shown in figure 8. Contrary to the 2.5 $\mu$m-diameter wire, it is not possible to obtain a square-wave response that looks like a classic optimal square-wave response for the 0.2 $\mu$m-diameter wire by changing offset voltage with this circuit. If just the electrical response is considered, one could conclude from the square-wave response of figure 8(a) that by increasing the offset voltage, the frequency response of the system increases. However this is disapproved by the transfer functions shown in figure 8(b). This test demonstrates

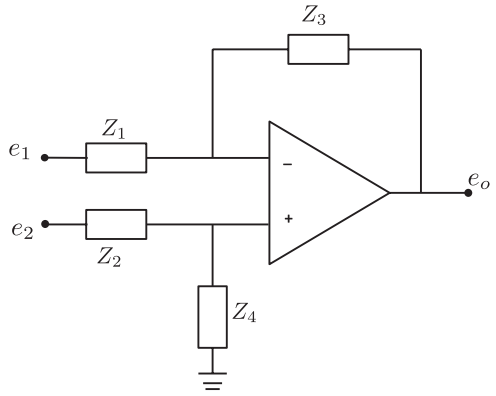


**Figure 13.** Circuit of a differential amplifier.

that square-wave tests can be misleading in operating a sub-miniature wire with a CTA designed for conventional hot-wires. In fact, in the transfer function of the CTA system in addition to the conjugate poles which are dominant in the conventional hot-wire case and create a second order peak in

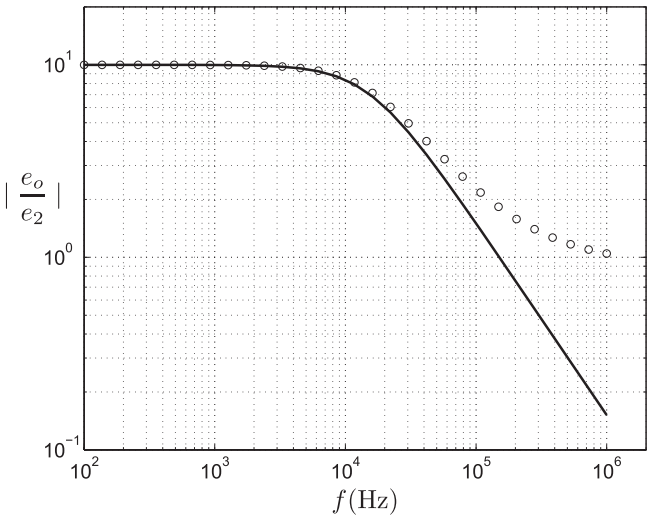


**Figure 14.** Magnitude of coefficient of $e_2$ (in equation (11)) for the amplifier circuit shown in figure 13 with capacitor in impedance $Z_4$ (——) and without capacitor in impedance $Z_4$(◦).

the transfer function, a simple pole is present which becomes significant for the 0.2 $\mu$m-diameter wire and becomes dominant by increasing offset voltage $E_{qi}$ and determines the real frequency response of the CTA system. This behaviour highlights the importance of analytical methods in finding the ideal response of sub-miniature hot-wires, which in turn requires sufficient information regarding the anemometer circuit and the hot-wire sensor heat transfer governing equation.

## 5. Operating sub-miniature wires: instability and breakage issues

Studying high-Reynolds number flows experimentally, requires very small sensors to avoid spatial averaging. This requirement has encouraged researchers to build sub-miniature sensors like the Princeton NSTAP [3]. Decreasing the dimensions of the sensor, increases its frequency response drastically; therefore, a high frequency response anemometer is required to operate it. Currently NSTAP can be safely controlled only with the Dantec Streamline anemometer with an external resistor. In this section the feasibility of using an anemometer based on the circuit given in figure 1 to operate sub-miniature probes is investigated with the aid of the theoretical model presented in section 2.

A MUCTA circuit with the following characteristics is simulated: a 10:1 ratio Wheatstone bridge with $R_a = 100\ \Omega$, $R_c = 1000\ \Omega$, and variable $R_b$ (and lumped inductance $L_b$) to adjust overheat ratio (and optimise frequency response). The first stage differential amplifier has a DC gain $K_a = 100$ and a single pole transfer function with cut-off frequency $f_c \approx 750$ kHz. The second stage amplifier is a differential amplifier having DC gain $K_b = 10$ and single pole transfer function with cut-off frequency $f_c \approx 15$ kHz.

Perry [1] and Watmuff [2] showed that the transfer functions related to both velocity and the square-wave test have the same poles. Moreover, a square-wave test is the only practical way to tune a CTA system and it usually provides a good representation of the system response to the velocity fluctuations; hence, to study the behaviour of the CTA system, the square-wave test transfer function (equation (7)) is investigated in this section.

Figure 9 shows the location of the dominant poles of the closed-loop transfer function related to the square-wave injection of the modelled CTA operating 5, 2.5, 1, 0.6, 0.3, and 0.12 $\mu$m-diameter wires on the s-plane. Lengths of the wires are 200 times their diameters, i.e. $l = 200d$. All wires have overheat ratios of 1.6 except for the 0.12 $\mu$m-diameter wire which has an overheat ratio of 1.3. Simple poles for 5, 2.5, 1, and 0.6 $\mu$m-diameter wires are far from the origin and cannot be seen in the figure. It can be seen that for the mentioned circuit characteristics, theory does not predict instability even for a 0.12 $\mu$m-diameter wire, since the poles are located in the left-half of the s-plane and reasonably far from imaginary axis. Figure 10 shows normalized transfer function magnitudes related to the square-wave test for the wires of figure 9. One can see that by decreasing the hot-wire size, the peak in the transfer function that corresponds to the square-wave frequency response of the CTA system moves to higher frequencies as expected, and for wires with diameters smaller than 0.6 $\mu$m, the frequency of the peak exceeds 300 kHz.

A 2.5 and 1 $\mu$m-diameter wire were tested with the MUCTA having circuit characteristics similar to the modelled anemometer to observe the system behaviour at higher frequencies more clearly. Their square-wave test transfer functions compared with model prediction are shown in figure 11. Like those of the 5 $\mu$m-diameter wire in figure 3, the experimental transfer functions deviate from theory at high frequencies for both the 2.5 and 1 $\mu$m-diameter wires. The magnitude of the transfer function at $f = 350$ kHz is approximately twice the theoretical magnitude for both wires. While it is not possible to precisely predict the effect of this deviation from theory for much smaller sub-miniature wires, a synthetic square-wave test transfer function and its corresponding time response for a 0.3 $\mu$m-diameter wire operated by the MUCTA at its current condition might be expected to resemble those shown in figure 12. The characteristic used to generate the synthetic transfer function shown in figure 12 is the ratio of the magnitude of the experimental transfer function to the magnitude of the theoretical transfer function at the expected peak of the 0.3 $\mu$m-diameter wire which is equal to this ratio for the tested 2.5 $\mu$m-diameter wire at the same frequency ($\approx$350 kHz). The resulting square-wave response is seen to be under-damped and close to instability. A fragile sub-miniature wire cannot survive such an oscillatory current passing through it and breaks immediately.

To find the reason for the discrepancy between theory and experiment, especially at high frequencies, all parts of the MUCTA circuit were reviewed and the second stage amplifier was found to be responsible for the near instability. Based on the theoretical model, it was determined that both amplifiers utilized in practice should be differential amplifiers in order for the circuit to comply with the theoretical analysis. The first amplifier should be an Instrumentation Amplifier since it amplifies very small differential signals of the Wheatstone

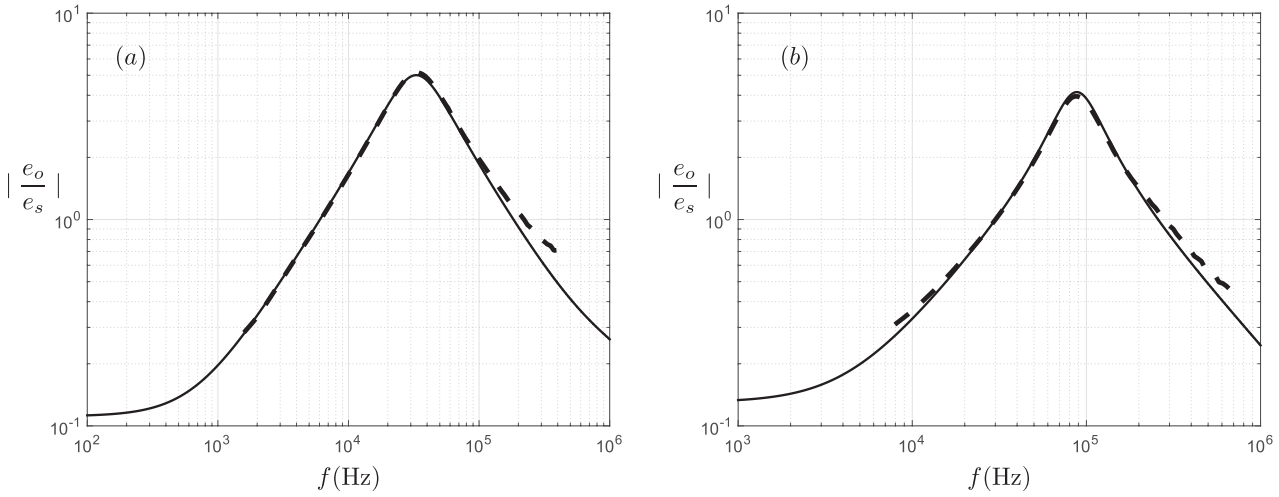


**Figure 15.** Comparison of theoretical and experimental transfer functions for square-wave test of the CTA system after adding the capacitor $C$ to the impedance $Z_4$ (in parallel to $R_4$). (a) 2.5 $\mu$m-diameter wire, (b) 1 $\mu$m-diameter wire. ——: theory, - - - -: experiment.

bridge, and the second amplifier can be constructed by a configuration as shown in figure 13 so that its DC gain and cut-off frequency can be controlled by choosing proper resistors and capacitors. In our anemometer circuit (figure 1), $e_1$ is the node connected to the output of the first amplifier and $e_2$ is the node connected to the offset voltage $E_{qi}$ (and square-wave test signal injection node). The transfer function for this configuration is given as

$$e_o = \left(\frac{Z_1 + Z_3}{Z_2 + Z_4} \times \frac{Z_4}{Z_1}\right)e_2 - \left(\frac{Z_3}{Z_1}\right)e_1 \tag{11}$$

If $Z_1 = Z_2$ and $Z_3 = Z_4$, equation (11) will reduce to

$$e_o = \frac{Z_3}{Z_1}(e_2 - e_1) \tag{12}$$

In practice it is not possible to have an infinitely flat amplifier response; therefore, the output of the second amplifier should be filtered at an appropriate frequency. To achieve this filtering, a capacitor $C$ is used in parallel with a resistor $R_3$ to form impedance $Z_3$. In that case and if $Z_1 = Z_2 = R_1$ and $Z_3 = Z_4$, the amplifier's relation will be

$$e_o = \frac{R_3}{R_1} \times \frac{1}{R_3 C s + 1}(e_2 - e_1) \tag{13}$$

If this capacitor is only applied in impedance $Z_3$, i.e. impedance $Z_4$ is just comprised of a resistor $R_4 = R_3$ (this is the case in the MUCTA circuit), the assumption that $Z_3 = Z_4$ will not be true for all frequencies and equation (12) or equivalently equation (13) cannot be used for the second amplifier. If we assume that resistors $R_1 = R_2$, $R_3 = R_4$ and capacitor $C$ are chosen such that $\frac{R_3}{R_1} = 10$ and $R_3 C \approx 10^{-5}$ s (as in MUCTA), the resulting magnitudes of coefficients of $e_2$ in equations (11) and (12) can be calculated. For these values, the magnitudes of the coefficients with and without inclusion of the capacitor $C$ in $Z_4$ are shown in figure 14 as a function of frequency $f$. It is interesting to notice that similar to figures 3 and 11, the curve corresponding to the amplifier without a capacitor in $Z_4$ peels off from the one corresponding to the amplifier with a capacitor in $Z_4$, and their difference accentuates as frequency increases. It

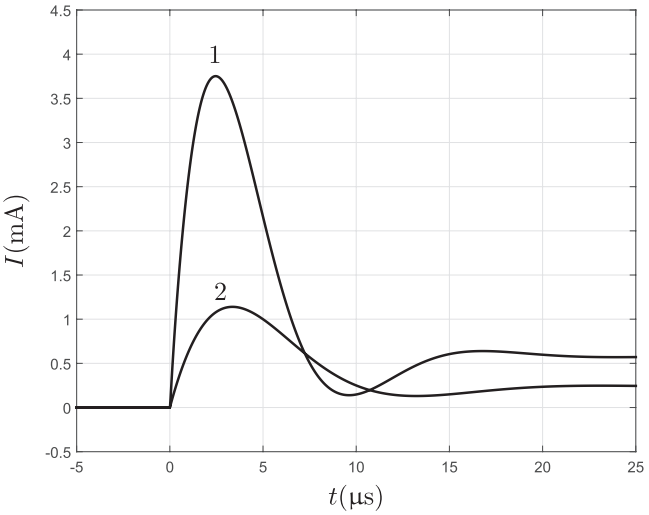


**Figure 16.** Electric current response of a 0.6 $\mu$m-diameter wire operated with simulated MUCTA to a 1 V step voltage signal injected to the offset voltage node. Two cases were simulated: 1-CTA circuit with $R_a = 100\ \Omega$ and $R_c = 1000\ \Omega$, 2-CTA circuit with $R_a = 1000\ \Omega$ and $R_c = 10\,000\ \Omega$.

should be noted that the mentioned difference between MUCTA and the theoretical square-wave transfer function is small for frequencies less than 100 kHz, hence it does not effect conventional hot-wire operations; furthermore, this capacitor does not impact the velocity fluctuations response since impedance $Z_4$ merely appears in the transfer function of node $e_2$ (see equation (11)) and during the velocity measurement $e_2 = 0$ since $e_2$ is connected to the square-wave test signal which is zero during the velocity measurement. For sub-miniature wires it will effect the square-wave response appearance (and anemometer tuning as a result) and also the stability of the square-wave test.

To solve the problem and force the MUCTA circuit to follow our theoretical model more faithfully, a capacitor equal to the one used in $Z_3$ was added to $Z_4$ (in parallel to $R_4$). The modified MUCTA was used to operate 2.5 and 1 $\mu$m-diameter wires with test conditions similar to those of figure 11 again. Transfer functions for sample square-wave tests are indicated

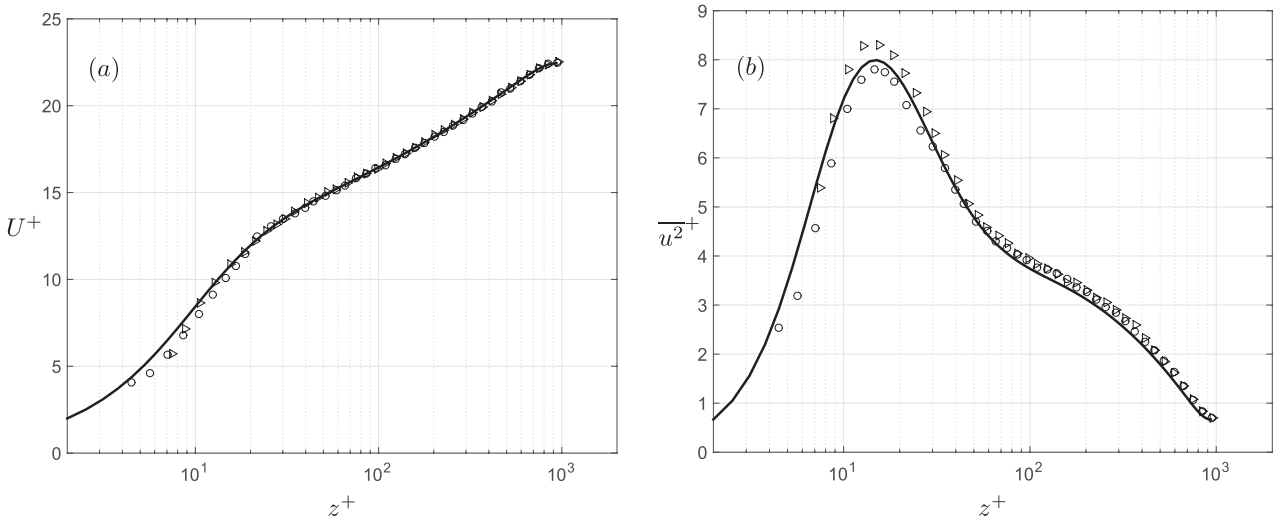


**Figure 17.** Comparison of the first and second order statistics, shown in the inner normalised coordinates. (a) Streamwise mean velocity ($U$) and (b) variance of streamwise velocity component ($\overline{u^2}$). ——: DNS, ◦: 2.5 $\mu$m-diameter wire results, and ▷: NSTAP results.

in figure 15. By comparing figures 11 and 15 one realizes that, after the modification, the match between MUCTA circuit and theory at high frequencies is significantly improved. However, the match is not still perfect which can be attributed to inaccurate capacitance measurement and/or the simple lumped model used for the wire.

The modified MUCTA circuit was used to operate NSTAP and a square-wave test was performed successfully to obtain an optimal square-wave response. However, frequent breakages during measurements persisted. Considering the fact that a stable square-wave response was obtained, breakage could not be due to instabilities alone. Fan *et al* [34] mention that excessive electric current can burn NSTAPs due to their small size compared with conventional wires (approximately 100 nm thickness compared to 5 $\mu$m diameter); therefore electric current fluctuations can damage them instantly. One way of dampening probable electric current fluctuations passing through NSTAP during operation is to increase the top-of-bridge resistors $R_a$ and $R_c$ [34]. MUCTA has been designed for conventional wires with a cold resistance of $R = \mathcal{O}(10)\ \Omega$ while the NSTAP cold resistance is $R = \mathcal{O}(100)\ \Omega$; therefore increasing the top-of-bridge resistors can help dampen electric current spikes which can burn-out the NSTAP. We tested this idea using the theoretical model by computing the current response of a 0.6 $\mu$m wire operated with simulated MUCTA to a 1 V step voltage signal injected to the offset voltage node. Two cases were simulated: (i) the CTA circuit with $R_a = 100\ \Omega$ and $R_c = 1000\ \Omega$, (ii) the same circuit but with $R_a = 1000\ \Omega$ and $R_c = 10\,000\ \Omega$. Results are depicted in figure 16. The peak electric current magnitude in the latter case is approximately 3 times smaller than the former case suggesting that for a given voltage fluctuation injected into the circuit, we can dampen electric current fluctuation magnitude by a factor of 3 in the MUCTA circuit by increasing the resistance of the top-of-bridge resistors by a factor of 10. Noting that for sub-miniature wires the static current during operation is on the order of milliamperes, one realises the importance of this difference. Convinced by theory, we changed the top-of-bridge resistors to $R_a = 1000\ \Omega$ and $R_c = 10\,000\ \Omega$ in MUCTA and after this modification successfully operated NSTAP for greatly extended periods with a much lower occurrence of breakage. We also noticed that after this modification the signal-to-noise ratio increased by a factor of approximately 3, i.e. for a given flow speed range past the NSTAP, the output voltage range became 3 times larger.

After applying both of the above-mentioned modifications, MUCTA was used to operate NSTAP at an overheat ratio $R = 1.3$ to measure streamwise velocity in the turbulent channel flow facility detailed in [35]. Mean velocity and associated broadband turbulence intensity profiles were measured using an NSTAP and a conventional 2.5 $\mu$m-diameter wire, and the results are presented in figure 17 where they are compared with DNS results from Hoyas and Jimenez [36] at comparable friction Reynolds number ($\mathrm{Re}_\tau = \frac{u_\tau h}{\nu} \approx 950$); here $u_\tau$ is friction velocity, $h$ is channel half-width, and $\nu$ is kinematic viscosity. In figure 17, $u$ denotes the streamwise fluctuating velocity, $z$ is wall-normal distance, and the superscript '+' indicates normalisation by inner variables. In this measurement the 2.5 $\mu$m-diameter wire has a non-dimensional length $l^+ = \frac{u_\tau l}{\nu} = 10$ where $l$ is active portion of the wire, while for NSTAP $l^+ = 1.2$. The mean velocity profiles are all seen to be in very good agreement, while the variance of streamwise velocity exhibits some small variations. The NSTAP results are seen to have higher peak turbulence levels as compared to the DNS. This behaviour has been formerly observed in pipe flow measurements when compared to DNS at relatively low Reynolds number $\mathrm{Re}_\tau \approx 3000$ [37]. This is likely because NSTAP is designed for high Reynolds number flow measurements, therefore its velocity sensitivity at low velocities is substantially less than conventional wires. Low sensitivity of NSTAP for very low velocities can be inferred from the calibration curve, where for velocities less than 2.5 $\mathrm{ms}^{-1}$ the slope of the calibration curve flattens out [19].

## 6. Summary and conclusions

An existing theoretical framework for CTAs that takes into account the finite frequency response of amplifiers in the feedback circuit was applied to analyse anemometry of sub-miniature hot-wires ($l < 100$ $\mu$m). Such probes are increasingly required for high Reynolds number turbulent flow measurements. Two transfer functions are developed by the theoretical analysis; one related to a circuit square-wave test and the other for velocity fluctuations. The accuracy of the model was assessed by modelling a MUCTA circuit. A 5 $\mu$m-diameter hot-wire was used for the assessment tests. The theoretical model compared well for the electrical fluctuations transfer function and fairly well for the velocity fluctuations transfer function when compared to experiment. A relative transfer function for velocity fluctuations was introduced since determining absolute experimental velocity transfer function up to high frequencies is not possible. Comparing theoretical relative velocity transfer functions to the experimental counterparts shows good qualitative agreement, although the model overestimates the cut-off frequency of the CTA, which is probably due to the simplified heat transfer model used for analysis of the hot-wire filament. Furthermore, the model was used to analyse operation of a sub-miniature hot-wire with a standard CTA designed to operate conventional hot-wires and revealed that the square-wave test could be misleading in showing true frequency response of the hot-wire-CTA system for sub-miniature wires.

A MUCTA circuit was further modelled to investigate the possibility of operating sub-miniature wires. With the aid of the model it was found that proper filtering of the second stage amplifier is required in order for MCUTA to perform the square-wave test with a sub-miniature wire, and the top-of-bridge resistors values, which are ideal for conventional wires, were found to be too small for NSTAP as even small electric current fluctuations can damage the sensor. By changing those resistors to 10 times the original values the fluctuations were dampened by a factor of 3 (as predicted by the theoretical model) and NSTAP wires were successfully operated by MUCTA. Using the modified CTA, NSTAP was used to measure velocity and turbulence profiles in a fully turbulent channel and these were compared with a 2.5 $\mu$m-diameter wire and DNS with very good observed agreement.

## Acknowledgments

The authors gratefully acknowledge Yuyang Fan and Dan Hoffman from Princeton University for their assistance, and the Australian Research Council for the financial support of this work.

## References

[1] Perry A E 1982 *Hot-Wire Anemometry* (New York: Oxford University Press)
[2] Watmuff J H 1995 An investigation of the constant-temperature hot-wire anemometer *Exp. Therm. Fluid Sci.* **11** 117–34
[3] Bailey S C, Kunkel G J, Hultmark M, Vallikivi M, Hill J P, Meyer K A, Tsay C, Arnold C B and Smits A J 2010 Turbulence measurements using a nanoscale thermal anemometry probe *J. Fluid Mech.* **663** 160–79
[4] Morrison J, McKeon B, Jiang W and Smits A 2004 Scaling of the streamwise velocity component in turbulent pipe flow *J. Fluid Mech.* **508** 99–131
[5] Österlund J M 1999 Experimental studies of zero pressure-gradient turbulent boundary layer flow *PhD thesis* Department of Mechanics, Royal Institute of Technology, Stockholm
[6] Nickels T, Marusic I, Hafez S and Chong M 2005 Evidence of the $k_1^{-1}$ law in a high-Reynolds-number turbulent boundary layer *Phys. Rev. Lett.* **95** 074501
[7] Carlier J and Stanislas M 2005 Experimental study of eddy structures in a turbulent boundary layer using particle image velocimetry *J. Fluid Mech.* **535** 143–88
[8] Vincenti P, Klewicki J, Morrill-Winter C, White C and Wosnik M 2013 Streamwise velocity statistics in turbulent boundary layers that spatially develop to high Reynolds number *Exp. Fluids* **54** 1–13
[9] Talamelli A, Persiani F, Fransson J H, Alfredsson P H, Johansson A V, Nagib H M, Rüedi J-D, Sreenivasan K R and Monkewitz P A 2009 Ciclope—a response to the need for high Reynolds number experiments *Fluid Dyn. Res.* **41** 021407
[10] Klewicki J C 2010 Reynolds number dependence, scaling, and dynamics of turbulent boundary layers *J. Fluids Eng.* **132** 094001
[11] Johansson A V and Alfredsson P H 1983 Effects of imperfect spatial resolution on measurements of wall-bounded turbulentbx shear flows *J. Fluid Mech.* **137** 409–21
[12] Willmarth W W and Sharma L K 1984 Study of turbulent structure with hot wires smaller than the viscous length *J. Fluid Mech.* **142** 121–49
[13] Ligrani P and Bradshaw P 1987 Spatial resolution and measurement of turbulence in the viscous sublayer using subminiature hot-wire probes *Exp. Fluids* **5** 407–17
[14] Hites M H 1997 Scaling of high-Reynolds number turbulent boundary layers in the National Diagnostic Facility *PhD thesis* Illinois Institute of Technology
[15] Hutchins N, Nickels T B, Marusic I and Chong M 2009 Hot-wire spatial resolution issues in wall-bounded turbulence *J. Fluid Mech.* **635** 103–36
[16] Jiang F, Tai Y-C, Ho C-M, Karan R and Garstenauer M 1994 Theoretical and experimental studies of micromachined hot-wire anemometers *Technical Digest., Int. Electron Devices Meeting* (IEEE) pp 139–42
[17] Marshall C, Matlis E, Corke T and Gogineni S 2015 AC plasma anemometer—characteristics and design *Meas. Sci. Technol.* **26** 085902
[18] Borisenkov Y, Gulitski G, Kholmyansky M, Krylov S, Liberzon A and Tsinober A 2015 Micro-machined super-miniature hot-film multi-array probe for field experiments with sub-kolmogorov resolution *J. Turbul.* **16** 525–39
[19] Vallikivi M and Smits A J 2014 Fabrication and characterization of a novel nanoscale thermal anemometry probe *J. Microelectromech. Syst.* **23** 899–907
[20] Freymuth P 1977 Frequency response and electronic testing for constant-temperature hot-wire anemometers *J. Phys. E: Sci. Instrum.* **10** 705
[21] Freymuth P 1967 Feedback control theory for constant-temperature hot-wire anemometers *Rev. Sci. Instrum.* **38** 677–81
[22] Perry A and Morrison G 1971 A study of the constant-temperature hot-wire anemometer *J. Fluid Mech.* **47** 577–99
[23] Wood N 1975 A method for determination and control of the frequency response of the constant-temperature hot-wire anemometer *J. Fluid Mech.* **67** 769–86

[24] Comte-Bellot G 1976 Hot-wire anemometry *Ann. Rev. Fluid Mech.* **8** 209–31
[25] Smits A, Perry A and Hoffmann P 1978 The response to temperature fluctuations of a constant-current hot-wire anemometer *J. Phys. E: Sci. Instrum.* **11** 909
[26] Morris S and Foss J 2003 Transient thermal response of a hot-wire anemometer *Meas. Sci. Technol.* **14** 251
[27] Li J 2004 Dynamic response of constant temperature hot-wire system in turbulence velocity measurements *Meas. Sci. Technol.* **15** 1835
[28] Li J 2005 The effect of electronic components on the cut-off frequency of the hot-wire system *Meas. Sci. Technol.* **16** 766
[29] Li J 2006 Dynamic response of constant temperature hot-wire systems under various perturbations *Meas. Sci. Technol.* **17** 2665
[30] Kramers H 1946 Heat transfer from spheres to flowing media *Physica* **12** 61–80
[31] Perry A and Morrison G 1971 Static and dynamic calibrations of constant-temperature hot-wire systems *J. Fluid Mech.* **47** 765–77
[32] Khoo B, Chew Y and Li G 1995 A new method by which to determine the dynamic response of marginally elevated hot-wire anemometer probes for near-wall velocity and wall shear stress measurements *Meas. Sci. Technol.* **6** 1399
[33] Hutchins N, Monty J, Hultmark M and Smits A 2015 A direct measure of the frequency response of hot-wire anemometers: temporal resolution issues in wall-bounded turbulence *Exp. Fluids* **56** 1–18
[34] Fan Y, Arwatz G, Van Buren T, Hoffman D and Hultmark M 2015 Nanoscale sensing devices for turbulence measurements *Exp. Fluids* **56** 1–13
[35] Monty J P 2005 Developments in smooth wall turbulent duct flows *PhD thesis* University of Melbourne, Australia
[36] Hoyas S and Jiménez J 2006 Scaling of the velocity fluctuations in turbulent channels up to $\mathrm{Re}_\tau = 2003$ *Phys. Fluids* **18** 011702
[37] Ahn J, Lee J H, Lee J, Kang J-H and Sung H J 2015 Direct numerical simulation of a 30R long turbulent pipe flow at $\mathrm{Re}_\tau = 3008$ *Phys. Fluids* **27** 065110